Title

Human Skeletal Muscle Myoblast Culture in Aligned Bacterial Nanocellulose and Commercial Matrices.

Journal

ACS Applied Materials & Interfaces, 16(36)

Authors

Mastrodimos, Melina
Jain, Saumya
Badv, Maryam
et al.

Publication Date

2024-09-11

DOI

10.1021/acsami.4c07612

Peer reviewed

ACS APPLIED MATERIALS & INTERFACES

www.acsami.org
Research Article

Human Skeletal Muscle Myoblast Culture in Aligned Bacterial Nanocellulose and Commercial Matrices

Melina Mastrodimos, Saumya Jain, Maryam Badv, Jun Shen, Hossein Montazerian, Claire E. Meyer, Nasim Annabi, and Paul S. Weiss*

Cite This: *ACS Appl. Mater. Interfaces* 2024, 16, 47150−47162

ABSTRACT: Bacterial nanocellulose (BNC) is a durable, flexible, and dynamic biomaterial capable of serving a wide variety of fields, sectors, and applications within biotechnology, healthcare, electronics, agriculture, fashion, and others. BNC is produced spontaneously in carbohydrate-rich bacterial culture media, forming a cellulosic pellicle via a nanonetwork of fibrils extruded from certain genera. Herein, we demonstrate engineering BNC-based scaffolds with tunable physical and mechanical properties through postprocessing. Human skeletal muscle myoblasts (HSMMs) were cultured on these scaffolds, and in vitro electrical stimulation was applied to promote cellular function for tissue engineering applications. We compared physiologic maturation markers of human skeletal muscle myoblast development using a 2.5-dimensional culture paradigm in fabricated BNC scaffolds, compared to two-dimensional (2D) controls. We demonstrate that the culture of human skeletal muscle myoblasts on BNC scaffolds developed under electrical stimulation produced highly aligned, physiologic morphology of human skeletal muscle myofibers compared to unstimulated BNC and standard 2D culture. Furthermore, we compared an array of metrics to assess the BNC scaffold in a rigorous head-to-head study with commercially available, clinically approved matrices, Kerecis Omega3 Wound Matrix (Marigen) and Phoenix as well as a gelatin methacryloyl (GelMA) hydrogel. The BNC scaffold outcompeted industry standard matrices as well as a 20% GelMA hydrogel in durability and sustained the support of human skeletal muscle myoblasts in vitro. This work offers a robust demonstration of BNC scaffold cytocompatibility with human skeletal muscle cells and sets the basis for future work in healthcare, bioengineering, and medical implant technological development.

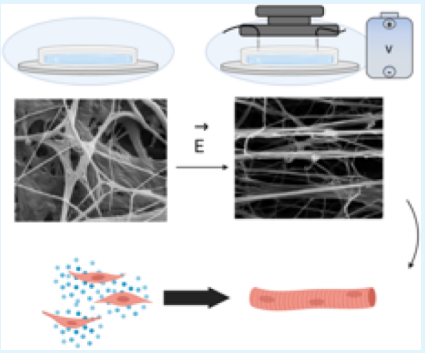

KEYWORDS: *bacterial nanocellulose, bioreactor, human skeletal muscle myoblasts, aligned, hydrogel, mesh, electrically stimulated, epitaxial, soft-tissue reconstruction*

INTRODUCTION

Bacterial nanocellulose (BNC) is an emerging biomaterial, with its chemical composition lending hydrophilicity and biodegradability, while being conducive to chemical modification.[1−5] During aerobic fermentation, BNC is produced as a cellulosic, gelatinous pellicle at the liquid−air interface of carbohydrate-rich media containing *Gluconacetobacter xylinum* or *Acetobacter xylinum*, as well as other genera.[4,6,7] Through continuous synthesis and deposition, *A. xylinum* and other synthetic species deposit a porous, webbed matrix of randomly oriented, pure cellulose.[8,9] Though cellulose produced by bacteria is chemically identical to plant cellulose, BNC is produced as a pure polymer and does not contain phytochemicals or immunogenic, pro-inflammatory contaminants (such as lignin, pectin, and hemicellulose).[8−13] Thus, compared to plant cellulose, no additional purification is necessary after BNC synthesis, highlighting several notable advantages. In addition, its porous structure leads to additional mechanical strength, a high Young's modulus, and additional water retention capacity compared to plant cellulose.[3,5,13]

Due to its durability, elasticity, and other physiologically relevant mechanical properties, BNC has been used as a promising biomaterial for culturing human skeletal muscle myoblasts (HSMMs) and other skeletal muscle-associated tissues.[14] Furthermore, BNC-based scaffolds have shown promise as a biomaterial for medical implants, as they have previously received significant attention as an absorptive bandage or dressing in wound healing due to their hydrophilicity, liquid retention capacity, and nontoxicity.[5,7,14−16] BNC also possesses unique physical and mechanical properties as a pure polymer, which can be tuned during and postsynthesis of the BNC pellicle fibers in vitro.[14,15,17,18]

Furthermore, numerous studies highlight the importance of hydrogel or scaffold patterning to direct myofiber development

Received: May 12, 2024
Revised: August 6, 2024
Accepted: August 6, 2024
Published: August 29, 2024

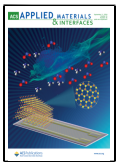

https://doi.org/10.1021/acsami.4c07612
ACS Appl. Mater. Interfaces 2024, 16, 47150−47162

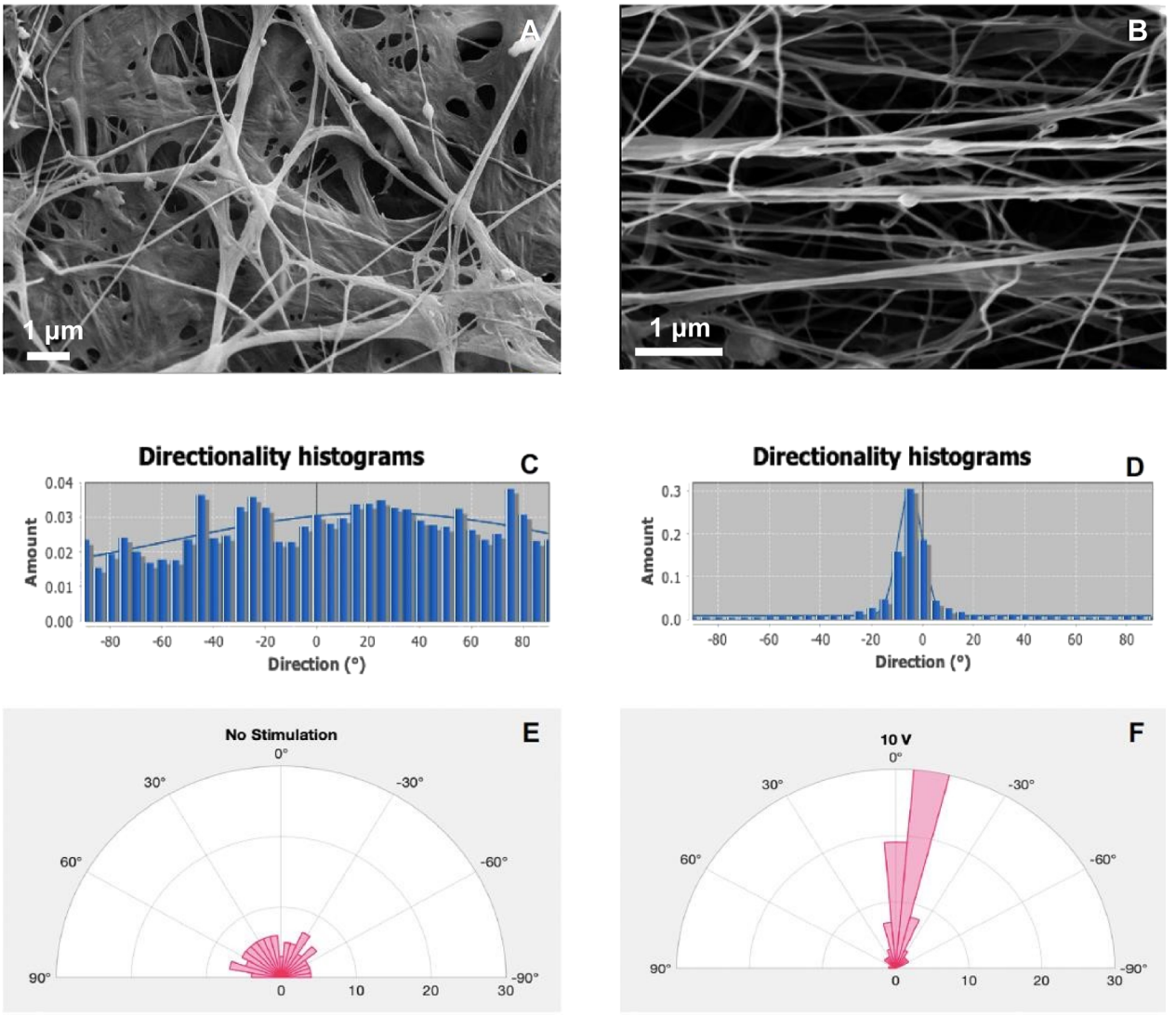

Figure 1. Scanning electron microscopy images of BNC under (A) control conditions (no stimulation) versus (B) electrical stimulation-mediated surface patterning of pellicles in vitro. (C,E) Histograms of control samples showed isotropic fiber orientations, while (D,F) histograms of electrically stimulated samples demonstrated anisotropic orientation with approximately 80% of fibers aligned between ±20° of the central axis. (E,F) Representative rose plots with BNC fiber orientations measured in 4° bins. A MATLAB script was utilized to determine the percentage of aligned fibers with permission and acknowledgment from Bolvar-Monsalve and Ceballos-Gonzáles.

in human and murine skeletal muscle tissue engineering models. BNC fiber orientation can be manipulated through an applied electric field to culture inoculum during in vitro synthesis.[12,19,20]

Drying methods have been shown to influence the structural and mechanophysical properties significantly, affecting properties, such as porosity and surface hornification, of BNC scaffolds.[1,4,21] Previous reports have achieved a spongy aerogel consistency through stepwise solvent exchange, critical point drying, and freeze-drying of BNC, which produce no significant changes in pellicle thicknesses and maintain a pliant dry aerogel with little brittleness. Reduced porosity and significant thickness reduction could be achieved through baking, producing compact, translucent sheets that are more brittle, yet still pliable.[1,21]

In this work, the effects of in vitro surface patterning and postprocessing drying methods on the properties of engineered BNC scaffolds are studied, specifically in the context of human skeletal muscle tissue engineering. We initially compare the traditional 2D well-plate cell culture of HSMMs with 2.5-dimensional (2.5D) cell culture of HSMMs seeded on BNC meshes. We further compared the 2.5D cell culture of HSMMs on BNC in a head-to-head comparison with commercially available matrices, Marigen and Pheonix, FDA-approved for wound healing indications, as a demonstration of biocompatibility and promise for applications in healthcare.[5,7,15,22] Here, we designed a custom bioreactor to deliver electric stimulation to BNC pellicles during late-stage incubation and synthesis, thus delivering uniaxial surface patterning to each pellicle through BNC fiber alignment.

Despite the ongoing research in this area and promising avenues of exploration, ideal surgical mesh materials are still being sought.[34] Meshes derived from biological materials typically have the best biocompatibility scores.[23,24] Decellularized biomaterials such as acellular dermal matrix are defined by chemical nontoxicity and a paucity of immunogenic epitopes. Implantation of these materials blunts the severity of any foreign body reactions marked by inflammation, edema, thrombosis, calcification, fibrosis, seroma formation, bowel adhesions,

https://doi.org/10.1021/acsami.4c07612
ACS Appl. Mater. Interfaces 2024, 16, 47150−47162

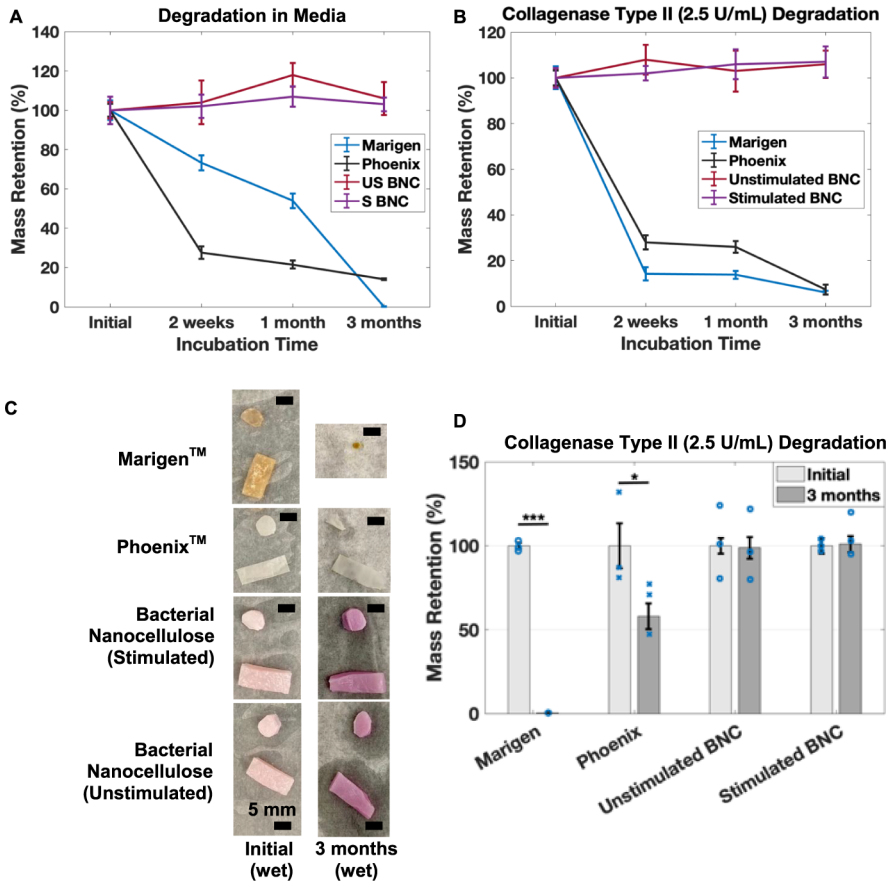

Figure 2. Bacterial nanocellulose versus commercial mesh performance evaluation. (A–D) Electrically stimulated bacterial nanocellulose (sBNC), unstimulated bacterial nanocellulose (usBNC) versus commercial Marigen and Phoenix matrices treated for up to three months under degradation conditions at 37 °C. (A,B) Effects of treatment on wet weight over all time points ($n = 5$). (D) Effects of treatment on dry weight at initial and final time points in the enzyme-treated degradation study. Enzyme treatment revealed partial degradation of Phoenix ($p < 0.05$) and near-total degradation of Marigen ($p < 0.0001$). (B–D) By comparison, BNC did not show signs of degradation by dry and wet weight under all experimental conditions. (A–D) Marigen degraded rapidly under enzyme treatment at 37 °C. (C) Optical photographic representation of (A) enzyme-free treatment and study revealing no signs of degradation in BNC after three-month incubation.

granuloma formation, and abscesses or fistulas.[23] While performance in antiinflammatory and cellular integration categories is excellent, many biologically derived materials lack durability, and are degraded or resorbed over time, highlighting limitations where permanent repair solutions are required.[25−27] In addition, materials such as an acellular dermal matrix used for surgical repair and tissue reconstruction are derived from cadavers and are thus unsustainable and costly. Therefore, there is significant interest in an ideal surgical mesh material with versatile physical and mechanical properties that also meets the rigorous requirements necessary for clinical use.

RESULTS AND DISCUSSION

Bacterial Nanocellulose Culture and Pellicle Harvesting. BNC was cultured in prepared media incubated at 26 °C and produced pellicles over the course of 3 weeks as previously described.[28] Bacterial nanocellulose is known to exhibit high moldability during fermentation as well as after material harvesting, and is highly responsive to different drying techniques.[1,17] Bacterial nanocellulose pellicles were either exposed to electrical stimulation or not subjected to such stimulation (as a control). After washing and decellularization, harvested pellicles were treated via oven drying, which produced thin, translucent sheets, while those processed via liquid nitrogen freeze-drying produced spongy aerogels.[17,21,28] Drying methods have implications for pore size as well as mechanical properties, which are dependent on liquid absorption capacity and water content in the wet state.[17] Higher liquid absorbance of BNC is associated with larger pore sizes at the baseline (evaluated via scanning electron microscopy (SEM) surface characterization), and lower Young's moduli.[17,29] Differing oven-dried or freeze-dried phenotypes and associated mechanophysical properties were produced in both electrically stimulated (surface-patterned) and unstimulated (control) BNC.

Scanning Electron Microscopy (SEM). As shown in Figure 1C,D, the microarchitecture of electrically stimulated BNC (sBNC) pellicles consisted of highly aligned fibers compared with control BNC (usBNC) pellicles grown under static culture conditions free of electric field implementation. Moreover, we observed greater than 80% uniaxial fiber alignment within ±20° of the axis midline after 10 V stimulation for 3 days in vitro (Figure 1E,F).

Electric field-stimulated BNC pellicles were decellularized, washed, and dried using either the liquid nitrogen freeze-drying or oven-drying protocol, then prepped for SEM imaging as described herein. Scanning electron microscopy images of sBNC samples were analyzed, and a MATLAB script was used to determine the fiber orientation order parameter (Figure 1E,F).[30]

https://doi.org/10.1021/acsami.4c07612
ACS Appl. Mater. Interfaces 2024, 16, 47150−47162

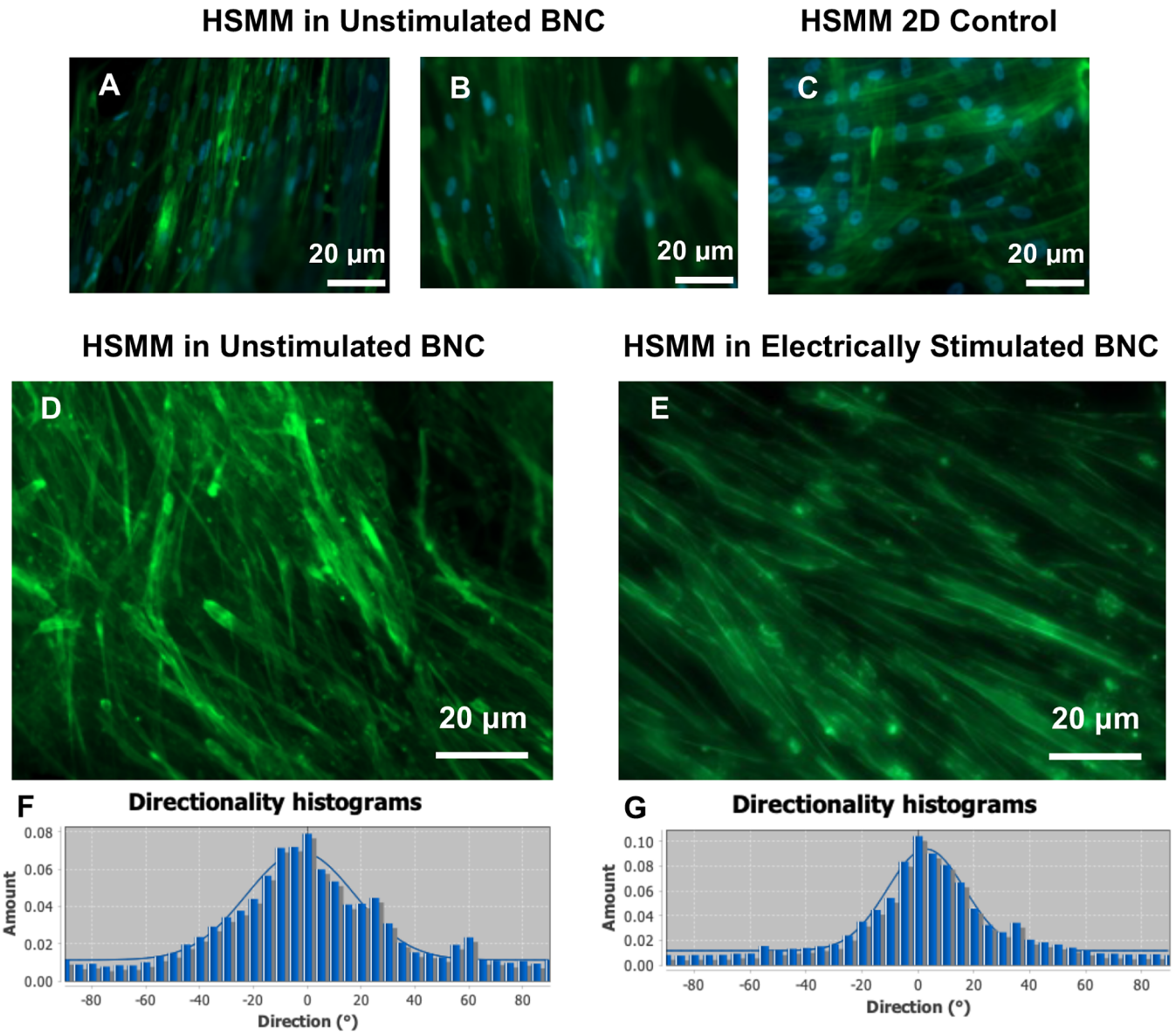

Figure 3. Fluorescence microscopy of a human skeletal muscle myoblast (HSMM) culture on bacterial nanocellulose (BNC). (A,B) Human skeletal muscle myoblast culture in BNC versus (C) 2D control. (A−C) Myofibers were stained for F-actin and nuclei, and (D,E) cellular integration (2.5-dimensional) into the mesh was achieved over approximately one month in culture. (D,E) Human skeletal muscle myoblast fluorescence microscopy in (D) unstimulated BNC and (E) electrically stimulated BNC. (D,E) Myofibers were stained for F-actin and cellular integration (2.5-dimensional) into the mesh was achieved over one month in culture to assess for alignment. Stained for F-actin. (F,G) Histograms of (D) and (E), respectively, reveal myofiber alignment with approximately half of the fibers aligned within ±20° of the central axis.

The image processing tool ImageJ (version 1.53t) was utilized to assess pore size in postprocessed BNC pellicles under our two drying protocols. As shown in Figure S1C,D,H, the distributions of pore sizes in the liquid nitrogen freeze-dried BNC pellicles possessed, on average, significantly larger pores (510 ± 38 nm) than pores in oven-dried BNC (230 ± 25 nm) pellicles ($p < 0.05$). Upon physical examination, oven-dried BNC pellicles were more translucent and had reduced thicknesses compared to liquid nitrogen freeze-dried pellicles (Figure S1A,B). Due to (1) the enhanced swelling capacity of liquid nitrogen freeze-dried BNC samples and (2) the mechanophysical equivalence between electrically stimulated and unstimulated freeze-dried samples, this drying protocol was implemented for cell culture investigations using sBNC versus commercial matrices.

Furthermore, to create BNC meshes readily compatible with physiological recapitulation and maintenance of human skeletal muscle morphology, we patterned the material through electrical stimulation of the BNC mesh in culture to produce aligned filaments, establish unilateral mesh anisotropy, and tune mesh porosity. To employ unilateral surface patterning, electrodes connected to a power source were placed in a culture to produce an electric field across the culture well, tube, or plate. The mesh material was subsequently patterned and synthesized in highly aligned filament arrays under these conditions, leading to a subsequent high-fidelity human skeletal muscle myofiber alignment when it was cultured on the patterned mesh. Unilateral surface patterning has important implications for implant performance when interfacing between distinct soft tissue subtypes, for example, parietal versus visceral tissue.[2,4]

Acellular dermal matrix preparations are utilized clinically to promote wound healing and as an adjunct in reconstructive surgeries.[22,23] Kerecis Omega3 (Marigen) Wound Matrix

https://doi.org/10.1021/acsami.4c07612
ACS Appl. Mater. Interfaces 2024, 16, 47150−47162

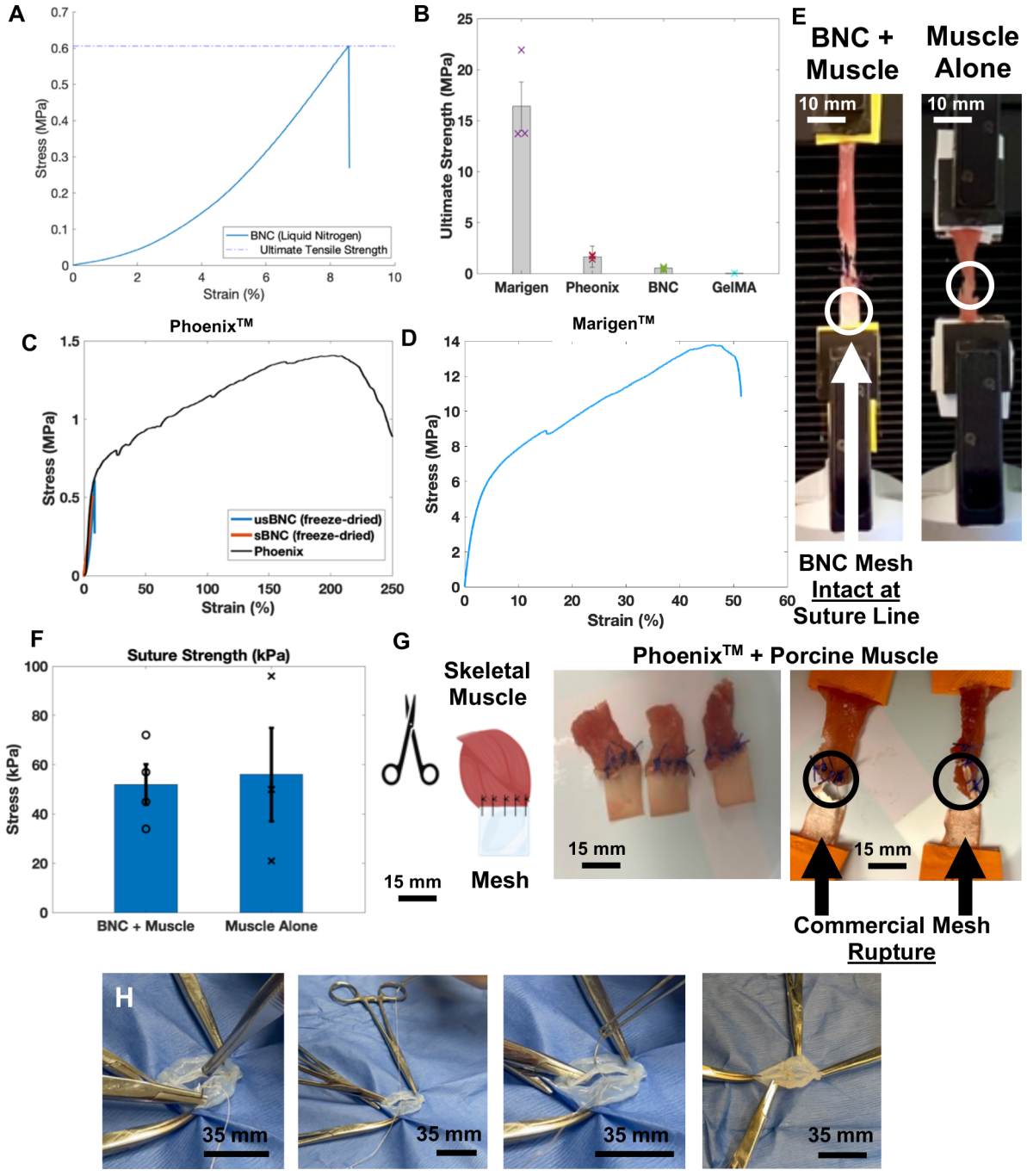

Figure 4. Mechanical characterization of candidate bacterial nanocellulose (BNC) matrix versus commercial samples. (A–D) Representative stress versus strain (%) graphs of liquid nitrogen freeze-dried BNC and commercial (Phoenix and Marigen) samples for Young's modulus and (B) ultimate strength evaluation. (E,F) Suture strength testing using bacterial nanocellulose sutured to the photographed (left, $n = 3$) porcine hindlimb muscle specimen and (right, $n = 3$) native porcine muscle specimen. Sutured samples were loaded into an Instron mechanical testing system and subjected to uniaxial strain until complete sample rupture occurred. (E,F) Suture strength testing of BNC-porcine muscle constructs performed similarly to muscle only controls. All BNC samples tested remained intact, and breakage occurred within the tissue with the majority of ruptures occurring along the suture line. (G) Representation of mesh suturing to the commercial Phoenix sample. (E,G) The majority of ruptures occurred within the commercial material, whereas none occurred in BNC-porcine muscle constructs. (H) Photographed BNC sample during clinical suturing demonstration. The figure was created with the assistance of BioRender.com.

(Kerecis, Isafjordur, Iceland) is an acellular dermal matrix of marine origin, derived from Atlantic cod skin and processed to retain the native protein (collagenous fiber) and matrix structure observed in the SEM images obtained (Figure S2B,E). The Phoenix commercial matrix is a proprietary polyester formulation produced from electrospinning, resulting in anisotropic fiber orientation with larger dry pore sizes (Figure S2C,F), in contrast to the fiber and pore morphologies observed for Marigen and usBNC in the SEM images shown in Figure S2A–F. Bacterial nanocellulose also demonstrated gross physical character similar to that of commercial meshes evaluated (Figure S2G).

Degradation Studies. Bacterial nanocellulose and commercial matrices were incubated at 37 °C for three months in

https://doi.org/10.1021/acsami.4c07612
ACS Appl. Mater. Interfaces 2024, 16, 47150–47162

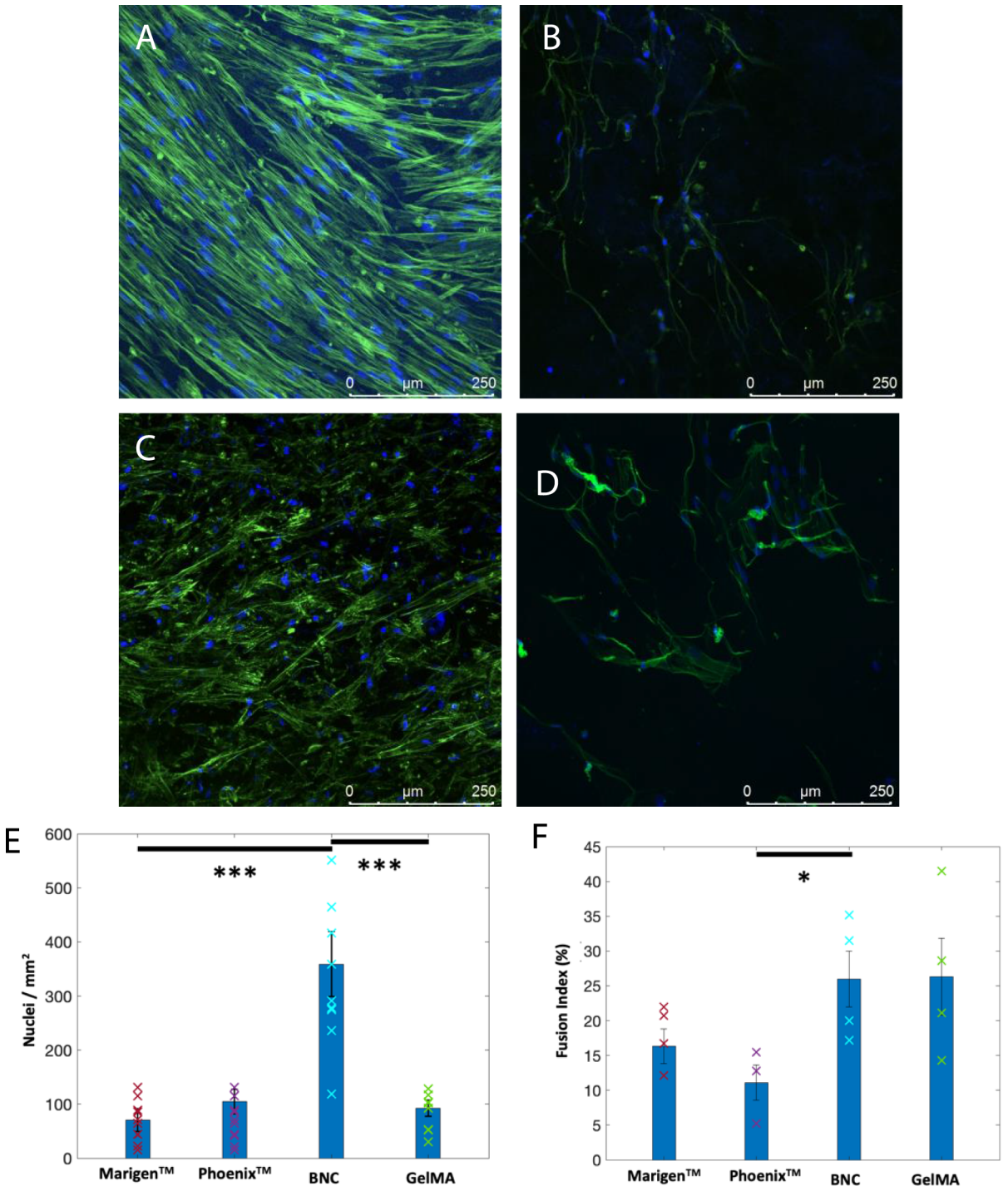

Figure 5. Representative confocal imaging of human skeletal muscle myoblasts in experimental and control matrices stained for F-actin and nuclei. (A) Endogenous ultrastructure is observed in representative bacterial nanocellulose constructs compared to representative (B) Marigen and (C) Phoenix commercial samples as well as (D) the gelatin methacryloyl traditional hydrogel. When cultured in electrically stimulated and aligned bacterial nanocellulose constructs, the myofiber alignment and nuclei count over one month were significantly improved over (B–D) other conditions. (E,F) Fusion index and nuclei counting in the 2.5D culture. Fusion indices and nuclei counting for each experimental and control sample for the one-month in vitro study period. Nuclei counting was completed using an ImageJ particle isolation and analysis protocol. Bacterial nanocellulose had significantly higher nuclei density per millimeter ($n = 9$) compared to all other samples. Fusion indices were comparable between bacterial nanocellulose cultures and gelatin methacryloyl (GelMA) control cultures but differed significantly from commercial sample cultures, Phoenix and Marigen.

media with or without 2.5 U/mL of collagenase type II (MMP-8) and analyzed over the study period (Figure 2A,B). Neither sBNC, nor usBNC, exhibited physical signs of degradation (Figure 2C). Comparatively, both commercial matrices revealed shrinkage and mass loss after the three-month in vitro incubation with enzyme, compared to BNC samples, which retained ca. 100% of their initial masses over the three-month period, as determined via wet and dry measurements (Figure 2A,B,D).

https://doi.org/10.1021/acsami.4c07612
ACS Appl. Mater. Interfaces 2024, 16, 47150−47162

When treated with high concentrations of protease (collagenase type II) and cellulase, BNC did not undergo wet mass change at 50 and 5 U/mL, but samples rapidly degraded in the presence of cellulase at both concentrations (1 and 10 mg/mL) to approximately 0% of initial mass as a positive control (Figure S3A,B). While not physiologically relevant, cellulase incubation demonstrates that BNC constructs are not impervious to enzyme treatment and can be selectively degraded. Bacterial nanocellulose also displayed no change in wet mass during the supraphysiological (up to 50 U/mL) enzyme incubation at 37 °C with MMP-8 over a five-day period (Figure S3B,D), demonstrating resistance to mass loss from the endogenous enzyme.

When subjected to a 37 °C incubation with and without MMP-8 for 5 days, Marigen underwent wet mass loss over the study period under both conditions (Figure S3C,D). Neither Phoenix nor BNC showed wet mass change in the in vitro incubation within 5 days; however, mass loss and degradation occurred in Phoenix samples after three months of incubation in collagenase type II extracellular matrix remodeling enzyme (2.5 U/mL) conditions in Figures S3C,D and 2B,D. Resistance to endogenous enzyme degradation suggests that BNC may be a promising candidate for permanent surgical mesh implantation, where durable, nonabsorbable soft-tissue reinforcement is clinically desired.

Both commercial matrices investigated herein are FDA-approved and were used as clinical comparators to BNC and 20% gelatin methacryloyl (GelMA) hydrogels in soft tissue biocompatibility (myoblast cytocompatibility) and mechanophysical parameters. Gelatin methacryloyl was incorporated based on its collagen-derived compositional similarities to Marigen. In the high concentration regime, GelMA hydrogels degraded completely by Day 3 when exposed to collagenase type II, similar to Marigen commercial samples (Figure S3D).

Cell Culture Studies. When HSMM 2.5D cultured in BNC was compared to a standard 2D culture, BNC constructs provided enhanced substrate suitability for the myofiber alignment compared to a standard well plate coated with Matrigel (Figure 3A−C). Similarly, HSMMs cultured in sBNC demonstrated enhancement of myofiber alignment compared with HSMMs in usBNC (Figure 3D−G). The majority of myofibers cultured in BNC samples were aligned within ±20° of the central axis (Figure 3D−G). The same image analysis technique was utilized for the myofiber alignment in BNC samples seeded with human skeletal muscle myoblasts.

Due to the favorable myofiber alignment in sBNC scaffolds and the observed mechanophysical similarities between sBNC and usBNC, electrically stimulated constructs were chosen for further investigation involving the HSMM culture (Figures 2A−D, 3D−G, and 4D). In aligned sBNC constructs, the enhanced myofiber alignment and markers of viability and maturity, including fusion indices, were observed compared to all other samples evaluated. Confocal microscopy revealed physiological-like morphology and ultrastructure in BNC samples over a one-month period in vitro (Figure 5A). While the BNC scaffold and GelMA hydrogel had high levels of HSMM proliferation at early time points and similar indices of myotube fusion and viability (fusion index) at one month, the BNC nuclei count of 350 ± 60 nuclei/mm^2 at the end of the study period was significantly higher than other samples, including commercial samples Phoenix and Marigen (104 ± 23 and 70 ± 20 nuclei/mm^2, respectively) and GelMA (93 ± 15 nuclei/mm^2) hydrogels (Figure 5E,F). Confocal imaging of the HSMM 2.5D culture in BNC versus GelMA revealed robust proliferation and highly aligned myofiber morphology in the aligned BNC experimental group (Figure 5A,B). Continued myofiber maintenance after one month in vitro in BNC is likely due to superior BNC scaffold durability and resistance to degradation compared to other samples evaluated (Figure 5A−D). For example, myoblasts grown in GelMA for over one month did not exhibit physiological morphology when analyzed via staining for signs of myofiber development, likely due to slow, ongoing degradation of the hydrogel in vitro (Figure 5D).

Previous methods of orienting cellulosic fibers have been employed in skeletal muscle tissue engineering to confer physiological myofiber alignment.[12,19,31−33] Plant-derived, decellularized cellulose scaffolds with anisotropic topography have shown promise in aligning murine C2C12 skeletal muscle myoblasts in a confluent layer, whereas isotropic, nonlinear patterning and variable topographic microgeometries have yielded less success.[12] Protein functionalization of cellulose scaffolds, as well as injectable, magnetic- or microfluidic-mediated alignment of BNC microfibrils, have also been investigated to promote myocyte adhesion and myofiber alignment.[2,31−35]

The surface patterning of the BNC mesh reported herein has important implications for tissue engineering, especially with respect to highly linearized tissue morphologies and ultrastructures exemplified in skeletal muscles, otherwise known as voluntary muscles.[12,20,36,37] Human skeletal muscles rely on linear organization for function and voluntary movement generation.[20,38,39] Human skeletal muscle tissue possesses natural regeneration capacity in response to minor stresses and injuries; through mechanisms under active investigation, a signaling cascade activates muscle stem cells (satellite cells) located within their niche, under the basal lamina along myofibers.[40] Severe muscle defects resulting in incomplete tissue regeneration in vivo from injury, denervation, ablation, infection debridement, or aggressive debulking surgeries can all cause functional deficits in patients and impact quality of life.[41−44]

Mechanical Properties. Young's moduli were calculated in the dry state for each material as Marigen samples were prone to breakage when wet. Gelatin methacryloyl samples were similarly weak and difficult to manipulate in the wet state. The Young's moduli of the samples were determined from the initial slope of the stress versus strain curve after performing a uniaxial tension test (Figures 4A,C−E, and S1F,G). As anticipated, there was batch-to-batch variability in the production of BNC mesh products and their respective mechanical properties. The postprocessing method also influenced BNC mechanical properties including tensile strength and hydroexpansivity in a tunable fashion with increased mechanical strength and decreased absorptive capacity attributed to oven drying with smaller pore sizes, as previously described (Figure S1C−E).[17,21,28]

Each experimental sample was readily manipulated and loaded into an Instron mechanical testing system for facile Young's modulus evaluation (Figure S4A−C). The Marigen commercial matrix showed the highest values (2.1 ± 0.24 MPa) in Figure 4B,D. By comparison, GelMA had the lowest Young's modulus (0.133 ± 0.003 kPa) by several orders of magnitude (Figure S4E). We also found that the Young's modulus of liquid nitrogen freeze-dried bacterial nanocellulose (0.103 ± 0.0365 MPa) was closest to that of Phoenix (0.15 ± 0.012 MPa) as shown in Figure 4A−C.

https://doi.org/10.1021/acsami.4c07612
ACS Appl. Mater. Interfaces 2024, 16, 47150−47162

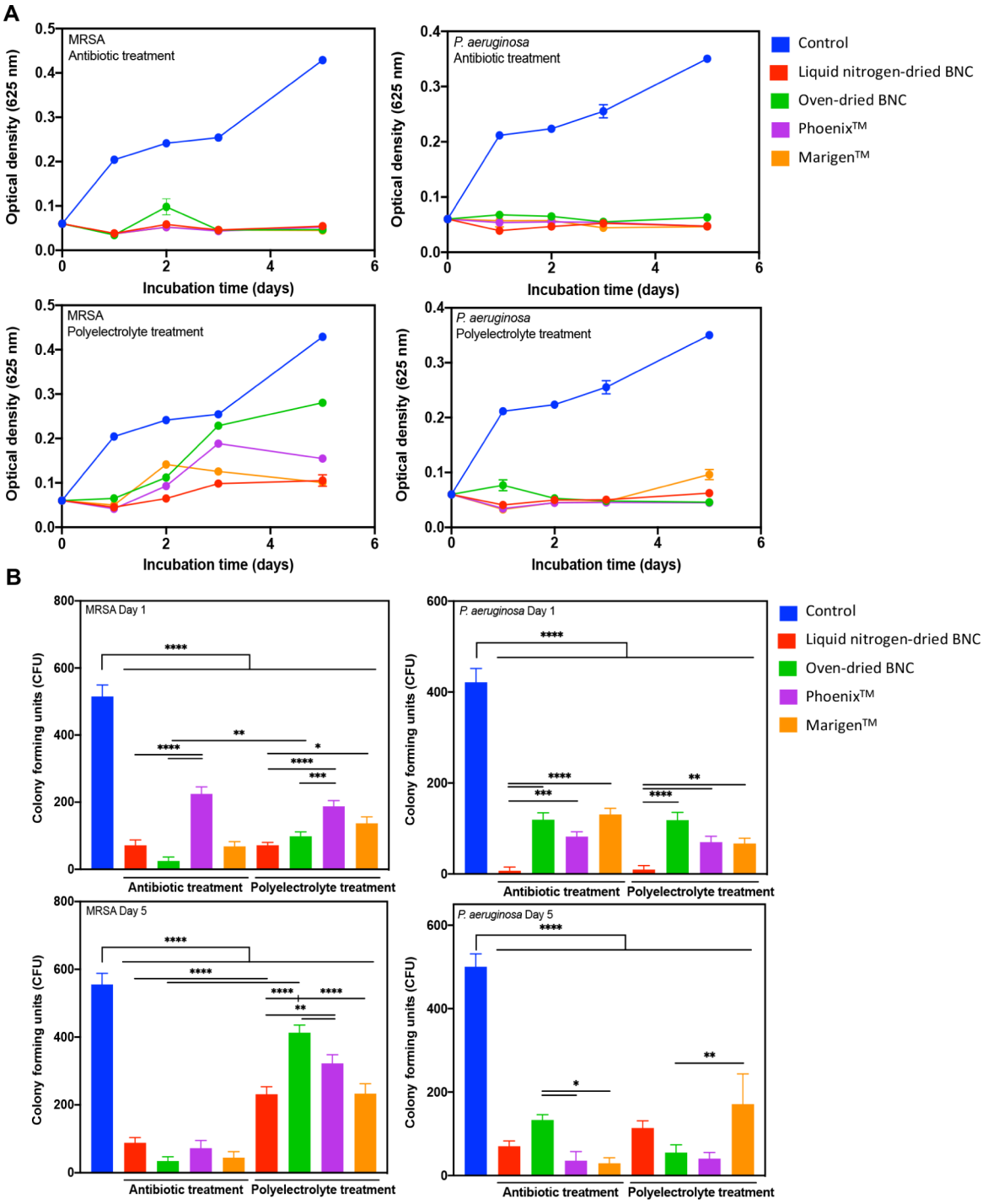

Figure 6. Antimicrobial loading and release assessment of bacterial nanocellulose (BNC) and commercial mesh products. Samples (n = 3) were incubated overnight in 2% broad spectrum antibiotic cocktail solution (doxycycline and ciprofloxacin) or 2% polyelectrolyte poly-(diallyldimethylammonium chloride) solution prior to inoculation and antimicrobial activity assessment against methicillin-resistant *Staphylococcus aureus* (MRSA) change and *Pseudomonas aeruginosa*. (A) Optical density as a proxy of bacterial concentration and (B) colony forming unit (cfu) measurements were performed over 5 days of bacterial incubation. (B) The highest cfu in the untreated control compared to all other drug-loaded samples ($p < 0.0001$) on Days 1−5.

The ultimate strength of liquid nitrogen freeze-dried samples was found to be 0.52 ± 0.14, while GelMA's ultimate strength was several orders of magnitude lower at 3.3 ± 1.5 kPa after one month (Figure 4B).

After one month, samples were collected for mechanical testing to investigate physical findings. Upon physical examination, GelMA hydrogels were comparatively difficult to handle and prone to breakage compared to BNC samples, which retained their character and physical integrity over the study period (Figure S4D,E).

Suture Strength. A clinical suturing demonstration was performed using BNC samples (Figure 4A and Video S1). Bacterial nanocellulose mesh samples were also compared to commercial Phoenix samples in the evaluation of suture strength

https://doi.org/10.1021/acsami.4c07612
ACS Appl. Mater. Interfaces 2024, 16, 47150−47162

(Figure 4F−I and Videos S2−S4). Suture strength was not evaluated in GelMA or Marigen samples as the samples were either too weak or too stiff to suture, respectively, in the dry state; GelMA or Marigen samples were both prone to breakage and not suturable in the wet state. All BNC samples sutured to porcine muscle remained intact, and the majority of ruptures occurred within the tissue at the suture line (Figure 4F). All samples demonstrated elastic and plastic deformation prior to rupture. In contrast to BNC sutured samples, the majority of Phoenix sutured samples ruptured within the commercial material matrix rather than in skeletal muscle tissue during testing (Figure 4F,I). Bacterial nanocellulose samples sutured to porcine muscles were also compared to native porcine muscle controls with no significant difference in the ultimate strength of native muscle versus muscle sutured to BNC (Figure 4F,G).

Antimicrobial Loading Capacity. Antibiotic and antimicrobial polyelectrolyte loading and bactericidal activity metrics in BNC mesh samples were compared with FDA-approved matrices (Marigen and Phoenix). Since swelling capacity was hypothesized to influence antimicrobial drug or polyelectrolyte loading capacity, both liquid nitrogen freeze-dried (aerogel-like) BNC and oven-dried BNC samples were included in the study (Figure 6A,B). The average cfu counts on Day 5 for liquid nitrogen freeze-dried BNC and oven-dried BNC were 88 ± 16 and 34 ± 13, respectively, for antibiotic treated samples. By comparison, the average cfu counts on Day 5 for Phoenix and Marigen were 72 ± 23 and 45 ± 18, respectively, treated under the same conditions. Control samples on Day 5 with no drug loading revealed significant bacterial growth over 5 days (Figure 6A,B). The average control cfu counts (555 ± 34) were significantly larger than both BNC drug-loaded sample types ($p < 0.0001$). The BNC antimicrobial drug loading was also improved compared to positive control glycidyl methacrylate-modified gelatin (GelMAG) cured with the poly(diallyldimethylammonium chloride) (pDDA) antimicrobial hydrogel (Figure 6B).

Tension-free anatomical repair using the mesh is regarded in many clinical settings as a superior option to direct suturing and tissue reanastomosis, particularly when reinforcing weak abdominal fascia in the setting of hernia surgery and repair. The surgical mesh for the hernia was implemented to reduce recurrence rates, which remained high (30−40%) when suturing the defect site under tension. This method was also associated with increased morbidity, as recurrent herniation was typically more severe, prone to infection, and often necessitated the administration of steroids. Thus, the introduction of surgical mesh is an engineering solution for primary suturing of hernia repair.[41−43]

Moreover, the mesh as a whole must possess antimicrobial activity or antibiotic loading capacity to reduce the risk of postoperative infection. Previous studies have indicated that parietal-facing versus viscera-facing differential porosity can assist with tissue integration and reduce the risk of bowel adhesion when the mesh is placed accordingly.

The effect of porosity also has important implications for the risk of biofilm development as a postsurgical complication of mesh implantation. Meshes with pores that are too small allow for the ingress of bacterial species but sterically blunt or hinder immune-mediated infiltration and surveillance of the implant. Mesh designs with submicron pores are particularly vulnerable and typically do not respond well to antibiotics once a biofilm is established.[45] Clinical management in these cases often necessitates hospital readmission, reoperation, mesh explantation, and local debridement.

CONCLUSIONS AND PROSPECTS

Despite batch-to-batch variations in development, each product met the capacity for support of HSMMs and the physical durability for our proposed healthcare indications. Bacterial nanocellulose constructs effectively maintained physiological myofibers compared to other conditions and materials tested, suggesting that BNC may be used as an implant material for skeletal muscle-associated soft tissue repair. Furthermore, to create BNC meshes readily compatible with physiological recapitulation and maintenance of human skeletal muscle morphology, we patterned the material through electrical stimulation of the BNC mesh in culture to produce aligned filaments, establish unilateral mesh anisotropy, and tune mesh porosity. To employ unilateral surface patterning, electrodes connected to a power source were placed in the culture to produce an electric field across the culture well, tube, or plate. The mesh material was subsequently patterned and synthesized in highly aligned filament arrays under these conditions, leading to a subsequent high-fidelity human skeletal muscle myofiber alignment when cultured on the patterned mesh. Specifically, the electrical alignment of BNC fibers produced in our scalable platform encouraged the physiological alignment of human myofibers in vitro compared to all other conditions evaluated. Unilateral surface patterning has important implications for implant performance when interfacing between distinct soft tissue subtypes, for example, parietal versus visceral tissue.[2,4] We also emphasize the utility of the high physiologic fidelity of our electrically aligned myofiber constructs using BNC, given the importance of the aligned myofiber ultrastructure in the physiological functionality of muscular soft tissues. This result suggests that BNC may be used as a permanent mesh implant to assist in tension-free surgical fixation and encourage physiological tissue development and mesh integration in the postoperative time course.

The implementation of permanent surgical meshes in soft tissue repair is instrumental in a myriad of reconstructive surgeries. Surgical mesh materials are often essential in hernioplasty, postmastectomy breast reconstruction, pelvic floor prolapse repair, duroplasty, and other surgical procedures.[14,25,46−48] In particular, hernioplasty is a common procedure performed in the setting of symptomatic soft-tissue herniation, a condition affecting more than 20 million people worldwide and with a lifetime risk of hernia of nearly one-third in men.[25,48]

The mainstay of hernia repair is tension-free fixation using a permanent surgical mesh. While this method is employed mainly to reduce the rate of hernia recurrence, next-generation approaches are necessary in order to improve upon current material products and solutions. Namely, mesh products must meet strict criteria including thresholds for tensile strength, biocompatibility, as well as prevention of infection, adhesions, and hernia recurrence.[25,27,48] We found that BNC exhibited robust mechanophysical properties as well as resistance to endogenous matrix metalloproteinase degradation, highlighting promise for permanent implantation and in vivo biomedical applications.[28]

EXPERIMENTAL METHODS

Materials. *Acetobacter xylinus* (ATCC 3767) was purchased through ATCC. SkBM-2 skeletal muscle myoblast basal medium and

https://doi.org/10.1021/acsami.4c07612
ACS Appl. Mater. Interfaces 2024, 16, 47150−47162

HSMM (CC-2580) were purchased from Lonza Bioscience. Gelatin from porcine skin (type A), methacrylic anhydride, and dopamine hydrochloride were supplied by Sigma-Aldrich. Sodium hydroxide (NaOH) pellets and dimethyl sulfoxide (DMSO) were purchased from Thermo Fisher Scientific. Glucose, yeast extract, bacto-peptone, NaH_2PO_4, citric acid, and photoinitiator 2-hydroxy-4′-(2-hydroxyethoxy)-2-methylpropiophenone (Irgacure 2959) were provided by Sigma-Aldrich. Dulbecco's phosphate-buffered saline (DPBS) was supplied by Thermo Fisher Scientific. Biopsy Punch, 6 mm (273692), was supplied by KRUUSE. The immunohistochemistry IgG anti-dystrophin antibody (Ab15277) was purchased through Abcam. Goat antirabbit Alexa-Fluor 568 (1:400; cat. no. 81-6114), phalloidin Alexa-Fluor 488 (1:1000; Invitrogen, cat. no, A12379), and DAPI (1 mg/mL) were purchased through Invitrogen.

Bacterial Nanocellulose Culture. The bacterial strain ATCC 3767 was selected for in vitro biosynthesis and production of BNC pellicles in our study. Here, we cultured BNC over the course of several weeks in prepared media. Bacterial culture media were prepared by mixing glucose (20 g L^{-1}), yeast extract (5 g L^{-1}), bacto-peptone (5 g L^{-1}), NaH_2PO_4 (2.7 g L^{-1}), and citric acid (1.5 g L^{-1}). The solution pH was adjusted to 5.0 and autoclaved for 45 min at 121 °C.[3,5]

Bacterial culture plates underwent multiple selection rounds to produce robust BNC pellicles. Briefly, the inoculum from productive wells during the first growth cycle of BNC was aspirated from liquid inferior to parental pellicles and seeded onto new plates with freshly prepared, warmed media at a ratio of 1:50. This selected inoculum stock was maintained in vitro for the duration of the study, and the inoculation procedure was repeated for each new growth cycle. The size of the pellicles could be tuned through well plate selection procedures, well plate size, and culture time prior to harvesting.

Apparatus was designed using AutoCAD Fusion 360 for electrical stimulation of BNC meshes in vitro using a standard power supply (Figure 1A). A custom-designed well plate lid was 3D printed using FormLabs Form3 printers and a biocompatible Surgical Guide resin. The lid was then retrofitted to a standard well plate, allowing for copper wire electrode incorporation into the tissue culture space for the establishment of voltage potentials across the well plate (Figure 1A,B).

After the establishment of BNC pellicles for 2 weeks in vitro in designed well plates, an electrical field was introduced for the remaining culture time. A potential of 10 V under direct current was applied across each well plate, and BNC pellicles were stimulated for a total of 3 days in vitro under a constant electric field in aqueous conditions.

After 3 weeks in culture at 26 °C, the BNC pellicles were harvested and washed with 1 M NaOH in a cleaning and decellularization step. Multiple wash out steps were pursued with DI water until the solution reached neutral pH for future work involving biological studies and materials.

Bacterial nanocellulose pellicles were then placed and stored in DI water at 4 °C in preparation for further processing. Washed and sterilized BNC underwent postprocessing for tuning mechanical and physical properties. Hydrated meshes underwent oven drying at 60 °C for 12 h on aluminum sheets. The remaining meshes were treated and processed via liquid nitrogen lyophilization. Meshes were submerged in liquid nitrogen and rapidly frozen until completely frozen stiff with care to avoid cracking. Meshes were then transported to a Labconco FreeZone 2.5 L -50C Benchtop Freeze Dryer and were lyophilized overnight. Oven-treated and freeze-dried meshes were then resterilized with UV radiation for 2 min prior to cell culture. Remaining meshes were autoclaved and sealed for biomedical applications.

Scanning Electron Microscopy. Analyses of the surface morphology were attained using an ultrahigh-resolution field emission gun scanning electron microscopy (SEM) instrument with an acceleration voltage of 10.0 kV (NOVA 200 Nano SEM; FEI, Hillsboro, OR, USA). To reduce perturbations in surface readouts from charge accumulation, BNC mesh samples were sputtercoated with a thin layer of gold−palladium under a nitrogen atmosphere (Agar Sputter Coater, PlanoGmbH).

Electric field-stimulated BNC pellicles were decellularized, washed, freeze-dried using the liquid nitrogen protocol, and then prepped for SEM imaging as described. SEM images of stimulated BNC samples were analyzed using ImageJ and a MATLAB script to determine the fiber orientation order parameter.[33] The same image analysis technique was used for myofiber alignment in sBNC samples versus usBNC samples seeded with human skeletal muscle myoblasts.

GelMA Synthesis. Dialyzed and freeze-dried GelMA was prepared as previously described.[49] Photocross-linking of GelMA was purused using the commercially available photoinitiator 2-hydroxy-1-[4-(2-hydroxyethoxy)phenyl]-2-methyl-1-propanone (Irgacure 2959) under aqueous conditions. Freeze-dried GelMA was dissolved in Milli-Q DI water. The solution was first heated to 50 °C for 10 min with the subsequent addition of photoinitiator Irgacure 2959. The warm aqueous 20% GelMA solution was placed in preformed molds designed and printed using AutoCAD Fusion 360 and FormLabs Form3 3D printers for photocross-linking with 0.5 wt % Irgacure 2959 under UV light (35 mW/cm^2) with an OmniCure Series 2000 Spot UV curing system (Excelitas Technologies) for 2 min.

Mechanical Testing. Sample stiffness was determined by applying a uniaxial tension test to cut 10 mm × 2 mm specimens. Tests were administered using an Instron 5943 Single Column Universal Testing System (Illinois Tool Works, Inc.) at room temperature. Samples were clamped at each end in the dynamic mechanical analysis instrument using two steel clamps and subjected to a uniaxial crosshead displacement rate of 4 mm/min. Testing was performed until a complete rupture occurred for each specimen.

Suture Strength. Suture strength testing was performed for BNC mesh samples secured to resected porcine hindlimb tissue. Biceps femoris tissue was resected from a previously frozen porcine hindlimb under meticulous surgical dissection. Biceps femoris tissue samples were then cut into 10 mm × 2 mm sections for suturing and mechanical evaluation. The inferior boundary of each porcine tissue sample was secured to the superior boundary of the sample mesh with five interrupted stitches using Ethicon 2−0 sutures and loaded onto an Instron Mechanical Testing System via glass slides for suture strength testing. Uniaxial crosshead displacement was pursued at a rate of 4 mm/min and proceeded until complete specimen rupture.

Degradation Studies. Samples were collected and weighed at each time point during the three-month degradation study, and solutions were replaced every 3 days. Degradation weights (wet and dry) were compared to initial wet and dry weights prior to in vitro incubation or in vitro incubation with enzyme treatment (Figure 2). Initial wet weights were defined and collected after overnight incubation at 4 °C to allow for full swelling and associated mass change.

Both BNC and commercial matrices were subjected to three-month in vitro conditions in the presence of the collagenase type II enzyme to assess degradation. Collagenase type II concentrations were selected to emulate physiological MMP-8 levels (Figure 2B,D).[50−53] Comparatively, supraphysiologic concentrations of MMP-8 (up to 50 U/mL) were also selected for further investigation (Figure S3A,B,D). Samples were placed in SkBM-2 skeletal muscle myoblast basal medium (Lonza Bioscience, CC-3246) prepared from the SkBM-2 skeletal muscle myoblasts basal medium bullet kit (Lonza Bioscience, CC-3246) and maintained at 37 °C for three months. Briefly, dry weights were collected for each sample prior to study initiation. Wet weights were determined after 24 h incubation at 4 °C and recorded at each time point during the study period. Final dry weights were recorded to assess degradation.

Furthermore, BNC and commercial samples were treated separately with two biological enzymes, collagenase type II (MMP-8) and cellulase, at 37 °C. Collagenase II was prepared at concentrations of 50, 5, and 2.5 U/mL in sterile-filtered 1% Dulbecco's phosphate buffered saline (Sigma-Aldrich). Cellulase was prepared at concentrations of 1 and 10 mg/mL in sterile-filtered Dulbecco's phosphate buffered saline (Sigma-Aldrich). Gelatin methacryloyl hydrogels were also treated under the same conditions. All samples were assessed for a total of 12 h in vitro under enzymatic treatment.

Cell Culture Studies. Stimulated BNC samples were compared to usBNC control samples, 20% GelMA hydrogels, commercial Marigen and Phoenix matrices, and traditional 2D culture. Specimens were cut into 6 mm disks using a KRUUSE Biopsy Punch, 6 mm (273692) prior to cell culture investigation. Disks were then sterilized with ethanol and

https://doi.org/10.1021/acsami.4c07612
ACS Appl. Mater. Interfaces 2024, 16, 47150−47162

allowed to dry; sterilized samples were placed in a 24-well plate in preparation for cell seeding. Each well was seeded with 200 000 human skeletal muscle myoblasts (Lonza Bioscience, CC-2580). Human skeletal muscle myoblast stock was first thawed and underwent multiple passages before cell seeding experiments between passages 4 and 7. Wells containing a 2D culture were first coated with Matrigel prior to cell seeding. Human skeletal muscle myoblasts were cultured using SkBM-2 skeletal muscle myoblast basal medium (Lonza Bioscience, CC-3246) prepared from SkBM-2 skeletal muscle myoblast basal medium bullet kit (Lonza Bioscience, CC-3246) over one month in vitro. Media were replaced every other day.

Fluorescence Microscopy. Samples from cell culture plates were harvested after one month and fixed for 20−30 min using a 4% paraformaldehyde solution. Fixed samples were then permeabilized in 0.1% Triton X-100 (Invitrogen) for 30 min and blocked in a 2% bovine serum albumin solution for 1−2 h. Cell staining for F-actin, nuclei, and dystrophin was performed according to the manufacturer's protocol. F-actin and nuclei were stained with phalloidin Alexa-Fluor 488 (1:1000; Invitrogen, cat. no. A12379) and DAPI (1 mg/mL). Dystrophin was stained with the Abcam IgG antidystrophin antibody (Ab15277). Secondary staining was performed with goat antirabbit Alexa-Fluor 568 (1:400; Invitrogen, cat. no. 81-6114). Fixed and stained samples were imaged using a Zeiss Observer fluorescence microscope.

Confocal Imaging. Human skeletal muscle myoblasts were seeded in electric field-stimulated and patterned BNC constructs, as well as 20% GelMA hydrogels and commercial Marigen and Phoenix matrices, with a seeding density of 100k cells/mL. Human skeletal muscle myoblasts were maintained in culture with SkBM-2 bullet kit media exchange every other day. Samples from cell culture plates were harvested after one month. Samples were fixed, permeabilized, and blocked using the aforementioned protocol and were then stained with F-actin, and nuclei were stained with phalloidin Alexa-Fluor 488 (1:1000; Invitrogen, cat. no. A12379) and DAPI (1 mg/mL). Samples were imaged using a STELLARIS 5 confocal microscope (Leica Microsystems) and assessed.

Antimicrobial Loading Capacity. All samples loaded with 2% antimicrobial polyelectrolyte or 2% broad-spectrum antibiotic exerted bacteriostatic activity. A measure of colony forming units (cfu) on Day 5 revealed equal antimicrobial activity between BNC and commercial samples. Samples were treated with 2% antimicrobial solution in bacterial culture broth and incubated with multidrug-resistant *S. aureus* (MRSA) or *P. aeruginosa* at an initial OD of 0.06 across all conditions. Liquid-nitrogen-dried and oven-dried BNC samples were compared to Phoenix and Marigen commercial samples as well as a GelMAG antimicrobial hydrogel positive control. Negative control wells contained bacteria with no hydrogel or matrix. To demonstrate drug loading, antimicrobial solutions were prepared using antibiotics (1% doxycycline and 1% ciprofloxacin) for broad-spectrum activity or 2% polyelectrolyte pDDA, which is often used in detergents.

To load either antibiotic agents, dry samples were incubated in 2% antimicrobial solution overnight at 4 °C to allow for maximum hydroexpansion and passive absorbance of antimicrobial solution into the sample matrix. Samples were also compared to hydrogels prepared with a polyelectrolyte solution loaded into the hydrogel matrix during curing with visible light (450−520 nm). Prior to inoculation with MRSA or *P. aeruginosa*, samples were UV sterilized for 2 min on each side at an intensity of 35 mW/cm^2 using an OmniCure Series 2000 Spot UV curing system (Excelitas Technologies).

After samples were treated with OD 0.06 bacterial suspension, they were incubated at 35 °C. At certain time points, suspended media were collected to assess bacterial survival through optical density measured in a microplate reader (BioTek Synergy). Suspended media were also diluted and plated on respective agar plates (tryptic soy broth for MRSA and lysogeny broth for *P. aeruginosa*) overnight at 35 °C. The next day, cfu were counted.

Statistics. Statistical differences between samples were calculated using a Student's two-tailed *t*-test or two-way ANOVA for independent readings or multiple comparisons, respectively.

■ ASSOCIATED CONTENT

Supporting Information

The Supporting Information is available free of charge at https://pubs.acs.org/doi/10.1021/acsami.4c07612.

Postprocessing differences in bacterial nanocellulose production yield physical variations in sample character and mechanophysical properties (Figure S1); scanning electron microscopy images of bacterial nanocellulose and commercial samples (Figure S2); degradation study comparing bacterial nanocellulose with gelatin methacryloyl and commercial samples (Figure S3); mechanical testing comparing bacterial nanocellulose with gelatin methacryloyl after one month of incubation (Figure S4) (PDF)

Bacterial nanocellulose reanastomosis and clinical suturing demonstration (Video S1) (MOV)

Bacterial nanocellulose suture strength testing (Video S2) (MP4)

Porcine muscle mechanical testing (Video S3) (MP4)

Commercial matrix suture strength testing (Video S4) (MP4)

■ AUTHOR INFORMATION

Corresponding Author

Paul S. Weiss − *California NanoSystems Institute, University of California, Los Angeles, Los Angeles, California 90095, United States; Department of Chemistry & Biochemistry and Department of Materials Science and Engineering, University of California, Los Angeles, Los Angeles, California 90095, United States; Department of Bioengineering, University of California, Los Angeles, Los Angeles, California 90095, United States;* orcid.org/0000-0001-5527-6248; Email: psw@cnsi.ucla.edu

Authors

Melina Mastrodimos − *California NanoSystems Institute, University of California, Los Angeles, Los Angeles, California 90095, United States; Department of Bioengineering, University of California, Los Angeles, Los Angeles, California 90095, United States;* orcid.org/0000-0002-2529-9577

Saumya Jain − *Department of Chemical and Biomolecular Engineering, University of California, Los Angeles, Los Angeles, California 90095, United States;* orcid.org/0009-0000-4080-4693

Maryam Badv − *Department of Biomedical Engineering, Schulich School of Engineering, University of Calgary, Calgary, Alberta T2N 1N4, Canada;* orcid.org/0000-0003-2226-3533

Jun Shen − *California NanoSystems Institute, University of California, Los Angeles, Los Angeles, California 90095, United States; Department of Chemistry & Biochemistry, University of California, Los Angeles, Los Angeles, California 90095, United States;* orcid.org/0000-0003-0383-6893

Hossein Montazerian − *California NanoSystems Institute, University of California, Los Angeles, Los Angeles, California 90095, United States; Department of Bioengineering, University of California, Los Angeles, Los Angeles, California 90095, United States; Terasaki Institute for Biomedical Innovation, Los Angeles, California 90024, United States;* orcid.org/0000-0001-6972-2667

https://doi.org/10.1021/acsami.4c07612
ACS Appl. Mater. Interfaces 2024, 16, 47150−47162

Claire E. Meyer − *Department of Chemistry & Biochemistry, University of California, Los Angeles, Los Angeles, California 90095, United States;* orcid.org/0000-0001-7258-9916

Nasim Annabi − *Department of Bioengineering, University of California, Los Angeles, Los Angeles, California 90095, United States; Department of Chemical and Biomolecular Engineering, University of California, Los Angeles, Los Angeles, California 90095, United States;* orcid.org/0000-0003-1879-1202

Complete contact information is available at: https://pubs.acs.org/10.1021/acsami.4c07612

Funding

This work was supported by the National Institutes of Health (NIH) Muscle Cell Biology, Pathophysiology, and Therapeutics T32 Training Grant (NIAMS #1T32AR065972), and the Challenge Initiative at UCLA.

Notes

The authors declare the following competing financial interest(s): M.M., M.B., and P.S.W. are inventors on patent applications filed by the Regents of the University of California relating to these materials and their applications.

■ ACKNOWLEDGMENTS

The authors acknowledge the support of the National Institutes of Health (NIH) Muscle Cell Biology, Pathophysiology, and Therapeutics T32 Training Grant, and the Challenge Initiative at UCLA. We thank Profs. Brigette Gomperts and Andrea Kasko for their helpful guidance and discussions. The authors gratefully thank Dr. Maxwell Wang for assistance in performing the clinical suturing demonstration.

■ REFERENCES

(1) Ul-Islam, M.; Khattak, W. A.; Kang, M.; Kim, S. M.; Khan, T.; Park, J. K. Effect of Post-Synthetic Processing Conditions on Structural Variations and Applications of Bacterial Cellulose. *Cellulose* **2013**, *20*, 253−263.

(2) Kuzmenko, V.; Sämfors, S.; Hägg, D.; Gatenholm, P. Universal Method for Protein Bioconjugation with Nanocellulose Scaffolds for Increased Cell Adhesion. *Mater. Sci. Eng., C* **2013**, *33*, 4599−4607.

(3) Lin, N.; Dufresne, A. Nanocellulose in Biomedicine: Current Status and Future Prospect. *Eur. Polym. J.* **2014**, *59*, 302−325.

(4) Klemm, D.; Cranston, E. D.; Fischer, D.; Gama, M.; Kedzior, S. A.; Kralisch, D.; Kramer, F.; Kondo, T.; Lindström, T.; Nietzsche, S.; et al. Nanocellulose as a Natural Source for Groundbreaking Applications in Materials Science: Today's State. *Mater. Today* **2018**, *21*, 720−748.

(5) Barja, F. Bacterial Nanocellulose Production and Biomedical Applications. *J. Biomed. Res.* **2021**, *35*, 310−317.

(6) Rangaswamy, B. E.; Vanitha, K. P.; Hungund, B. S. Microbial Cellulose Production from Bacteria Isolated from Rotten Fruit. *Int. J. Polym. Sci.* **2015**, *2015*, 280784.

(7) Ahmed, J.; Gultekinoglu, M.; Edirisinghe, M. Bacterial Cellulose Micro-Nano Fibres for Wound Healing Applications. *Biotechnol. Adv.* **2020**, *41*, 107549.

(8) McNamara, J. T.; Morgan, J. L. W.; Zimmer, J. A Molecular Description of Cellulose Biosynthesis. *Annu. Rev. Biochem.* **2015**, *84*, 895−921.

(9) Jacek, P.; Dourado, F.; Gama, M.; Bielecki, S. Molecular Aspects of Bacterial Nanocellulose Biosynthesis. *Microb. Biotechnol.* **2019**, *12*, 633−649.

(10) Keegstra, K. Plant Cell Walls. *Plant Physiol.* **2010**, *154*, 483−486.

(11) Guerriero, G.; Fugelstad, J.; Bulone, V. What Do We Really Know about Cellulose Biosynthesis in Higher Plants? *J. Integr. Plant Biol.* **2010**, *52*, 161−175.

(12) Cheng, Y.-W.; Shiwarski, D. J.; Ball, R. L.; Whitehead, K. A.; Feinberg, A. W. Engineering Aligned Skeletal Muscle Tissue Using Decellularized Plant-Derived Scaffolds. *ACS Biomater. Sci. Eng.* **2020**, *6*, 3046−3054.

(13) Delmer, D. P. Cellulose Biosynthesis: Exciting Times for A Difficult Field of Study. *Annu. Rev. Plant. Physiol. Plant. Mol. Biol.* **1999**, *50*, 245−276.

(14) Zwirner, J.; Ondruschka, B.; Scholze, M.; Schulze-Tanzil, G.; Hammer, N. Biomechanical Characterization of Human Temporal Muscle Fascia in Uniaxial Tensile Tests for Graft Purposes in Duraplasty. *Sci. Rep.* **2021**, *11*, 2127.

(15) Pang, M.; Huang, Y.; Meng, F.; Zhuang, Y.; Liu, H.; Du, M.; Ma, Q.; Wang, Q.; Chen, Z.; Chen, L.; et al. Application of Bacterial Cellulose in Skin and Bone Tissue Engineering. *Eur. Polym. J.* **2020**, *122*, 109365.

(16) Picheth, G. F.; Pirich, C. L.; Sierakowski, M. R.; Woehl, M. A.; Sakakibara, C. N.; Souza, C. F. D.; Martin, A. A.; Silva, R. D.; Freitas, R. A. D. Bacterial Cellulose in Biomedical Applications: A Review. *Int. J. Biol. Macromol.* **2017**, *104*, 97−106.

(17) Andree, V.; Niopek, D.; Müller, C.; Eiselt, J.-P.; Foh, N.; Rzany, A.; Hensel, B. Influence of Drying Methods on the Physical Properties of Bacterial Nanocellulose. *Mater. Res. Express* **2021**, *8*, 025402.

(18) Singh, G.; Chanda, A. Mechanical Properties of Whole-Body Soft Human Tissues: A Review. *Biomed. Mater. Bristol Engl.* **2021**, *16*, 062004.

(19) Sano, M. B.; Rojas, A. D.; Gatenholm, P.; Davalos, R. V. Electromagnetically Controlled Biological Assembly of Aligned Bacterial Cellulose Nanofibers. *Ann. Biomed. Eng.* **2010**, *38*, 2475−2484.

(20) Reid, G.; Magarotto, F.; Marsano, A.; Pozzobon, M. Next Stage Approach to Tissue Engineering Skeletal Muscle. *Bioeng. Basel Switz.* **2020**, *7*, 118.

(21) Bodea, I. M.; Beteg, F. I.; Pop, C. R.; David, A. P.; Dudescu, M. C.; Vilău, C.; Stănilă, A.; Rotar, A. M.; Cătunescu, G. M. Optimization of Moist and Oven-Dried Bacterial Cellulose Production for Functional Properties. *Polymers* **2021**, *13*, 3821.

(22) Dorweiler, B.; Trinh, T. T.; Dünschede, F.; Vahl, C. F.; Debus, E. S.; Storck, M.; Diener, H. The Marine Omega3 Wound Matrix for Treatment of Complicated Wounds: A Multicenter Experience Report. *Gefässchirurgie* **2018**, *23* (Suppl 2), 46−55.

(23) du Plessis, M. I.; Cottler, P. S.; Campbell, C. A. Acellular Dermal Matrix Favorably Modulates the Healing Response after Surgery. *Plast. Reconstr. Surg.* **2022**, *150*, 290e−299e.

(24) Boso, D.; Maghin, E.; Carraro, E.; Giagante, M.; Pavan, P.; Piccoli, M. Extracellular Matrix-Derived Hydrogels as Biomaterial for Different Skeletal Muscle Tissue Replacements. *Mater. Basel Switz.* **2020**, *13*, 2483.

(25) Deeken, C. R.; Faucher, K. M.; Matthews, B. D. A Review of the Composition, Characteristics, and Effectiveness of Barrier Mesh Prostheses Utilized for Laparoscopic Ventral Hernia Repair. *Surg. Endosc.* **2012**, *26*, 566−575.

(26) Ghanashyam, A.; Cryatal, S. S.; Glenn, S. B.; Jose, C. F. Multifunctional Biomesh for Surgical Hernia Repair, US 20,220,192,811 A1, 2022. https://lens.org/073-606-828-979-461.

(27) Koscielny, A.; Widenmayer, S.; May, T.; Kalff, J.; Lingohr, P. Comparison of Biological and Alloplastic Meshes in Ventral Incisional Hernia Repair. *Langenbecks Arch. Surg.* **2017**, *403*, 255−263.

(28) Roberts, E. L.; Abdollahi, S.; Oustadi, F.; Stephens, E. D.; Badv, M. Bacterial-Nanocellulose-Based Biointerfaces and Biomimetic Constructs for Blood-Contacting Medical Applications. *ACS Mater. Au* **2023**, *3*, 418−441.

(29) Fernandes, M.; Gama, M.; Dourado, F.; Souto, A. P. Development of Novel Bacterial Cellulose Composites for the Textile and Shoe Industry. *Microb. Biotechnol.* **2019**, *12*, 650−661.

(30) Bolívar-Monsalve, E. J.; Ceballos-González, C. F.; Borrayo-Montaño, K. I.; Quevedo-Moreno, D. A.; León, J. F. Y.; Khademhosseini, A.; Weiss, P. S.; Alvarez, M. M.; Santiago, G. T. Continuous Chaotic Bioprinting of Skeletal Muscle-Like Constructs. *Bioprinting* **2021**, *21*, No. e00125.

(31) De France, K. J.; Yager, K. G.; Chan, K. J. W.; Corbett, B.; Cranston, E. D.; Hoare, T. Injectable Anisotropic Nanocomposite Hydrogels Direct *in Situ* Growth and Alignment of Myotubes. *Nano Lett.* **2017**, *17*, 6487−6495.
(32) Dugan, J. M.; Gough, J. E.; Eichhorn, S. J. Directing the Morphology and Differentiation of Skeletal Muscle Cells Using Oriented Cellulose Nanowhiskers. *Biomacromolecules* **2010**, *11*, 2498−2504.
(33) Chen, C.; Zhang, T.; Dai, B.; Zhang, H.; Chen, X.; Yang, J.; Liu, J.; Sun, D. Rapid Fabrication of Composite Hydrogel Microfibers for Weavable and Sustainable Antibacterial Applications. *ACS Sustainable Chem. Eng.* **2016**, *4*, 6534−6542.
(34) Quero, F.; Quintro, A.; Orellana, N.; Opazo, G.; Mautner, A.; Jaque, N.; Valdebenito, F.; Flores, M.; Acevedo, C. Production of Biocompatible Protein Functionalized Cellulose Membranes by a Top-Down Approach. *ACS Biomater. Sci. Eng.* **2019**, *5*, 5968−5978.
(35) Domingues, R. M. A.; Gomes, M. E.; Reis, R. L. The Potential of Cellulose Nanocrystals in Tissue Engineering Strategies. *Biomacromolecules* **2014**, *15*, 2327−2346.
(36) Chen, S.; Nakamoto, T.; Kawazoe, N.; Chen, G. Engineering Multi-Layered Skeletal Muscle Tissue by Using 3D Microgrooved Collagen Scaffolds. *Biomaterials* **2015**, *73*, 23−31.
(37) An, Y.; Li, D. Engineering Skeletal Muscle Tissue in Bioreactor Systems. *Chin Med. J.* **2014**, *127*, 4130−4139.
(38) Feinberg, A. W.; Alford, P. W.; Jin, H.; Ripplinger, C. M.; Werdich, A. A.; Sheehy, S. P.; Grosberg, A.; Parker, K. K. Controlling the Contractile Strength of Engineered Cardiac Muscle by Hierarchal Tissue Architecture. *Biomaterials* **2012**, *33*, 5732−5741.
(39) Tamargo, M. A.; Nash, T. R.; Fleischer, S.; Kim, Y.; Vila, O. F.; Yeager, K.; Summers, M.; Zhao, Y.; Lock, R.; Chavez, M.; et al. milliPillar: A Platform for the Generation and Real-Time Assessment of Human Engineered Cardiac Tissues. *ACS Biomater. Sci. Eng.* **2021**, *7*, 5215−5229.
(40) Yin, H.; Price, F.; Rudnicki, M. A. Satellite Cells and the Muscle Stem Cell Niche. *Physiol. Rev.* **2013**, *93*, 23−67.
(41) Choi, Y.-J.; Jun, Y.-J.; Kim, D. Y.; Yi, H.-G.; Chae, S.-H.; Kang, J.; Lee, J.; Gao, G.; Kong, J.-S.; Jang, J.; et al. A 3D Cell Printed Muscle Construct with Tissue-Derived Bioink for the Treatment of Volumetric Muscle Loss. *Biomaterials* **2019**, *206*, 160−169.
(42) Corona, B. T.; Wenke, J. C.; Ward, C. L. Pathophysiology of Volumetric Muscle Loss Injury. *Cells Tissues Organs* **2016**, *202*, 180−188.
(43) Grasman, J. M.; Zayas, M. J.; Page, R. L.; Pins, G. D. Biomimetic Scaffolds for Regeneration of Volumetric Muscle Loss in Skeletal Muscle Injuries. *Acta Biomater.* **2015**, *25*, 2−15.
(44) Grogan, B. F.; Hsu, J. R. Volumetric Muscle Loss. *J. Am. Acad. Orthop. Surg.* **2011**, *19 Suppl. 1*, S35−S37.
(45) Wilson, R. B.; Farooque, Y. Risks and Prevention of Surgical Site Infection after Hernia Mesh Repair and the Predictive Utility of ACS-NSQIP. *J. Gastrointest. Surg. Off. J. Soc. Surg. Aliment. Tract* **2022**, *26*, 950−964.
(46) Afonso, J. S.; Martins, P. A. L. S.; Girao, M. J. B. C.; Natal Jorge, R. M.; Ferreira, A. J. M.; Mascarenhas, T.; Fernandes, A. A.; Bernardes, J.; Baracat, E. C.; Rodrigues de Lima, G.; et al. Mechanical Properties of Polypropylene Mesh Used in Pelvic Floor Repair. *Int. Urogynecology J.* **2008**, *19*, 375−380.
(47) Aghaei-Ghareh-Bolagh, B.; Mukherjee, S.; Lockley, K. M.; Mithieux, S. M.; Wang, Z.; Emmerson, S.; Darzi, S.; Gargett, C. E.; Weiss, A. S. A Novel Tropoelastin-Based Resorbable Surgical Mesh for Pelvic Organ Prolapse Repair. *Mater. Today Bio* **2020**, *8*, 100081.
(48) Alkhoury, F.; Helton, S.; Ippolito, R. J. Cost and Clinical Outcomes of Laparoscopic Ventral Hernia Repair Using Intraperitoneal Nonheavyweight Polypropylene Mesh. *Surg. Laparosc. Endosc. Percutan. Technol.* **2011**, *21*, 82−85.
(49) Van Den Bulcke, A. I.; Bogdanov, B.; De Rooze, N.; Schacht, E. H.; Cornelissen, M.; Berghmans, H. Structural and Rheological Properties of Methacrylamide Modified Gelatin Hydrogels. *Biomacromolecules* **2000**, *1*, 31−38.
(50) Nwomeh, B. C.; Liang, H. X.; Cohen, I. K.; Yager, D. R. MMP-8 Is the Predominant Collagenase in Healing Wounds and Nonhealing Ulcers. *J. Surg. Res.* **1999**, *81*, 189−195.
(51) Najafi, M.; Asadi, H.; van den Dikkenberg, J.; van Steenbergen, M. J.; Fens, M. H. A. M.; Hennink, W. E.; Vermonden, T. Conversion of an Injectable MMP-Degradable Hydrogel into Core-Cross-Linked Micelles. *Biomacromolecules* **2020**, *21*, 1739−1751.
(52) Zucker, S.; Doshi, K.; Cao, J. Measurement of Matrix Metalloproteinases (MMPs) and Tissue Inhibitors of Metalloproteinases (TIMP) in Blood and Urine: Potential Clinical Applications. *Adv. Clin. Chem.* **2004**, *38*, 37−85.
(53) Saleh, B.; Dhaliwal, H. K.; Portillo-Lara, R.; Shirzaei Sani, E.; Abdi, R.; Amiji, M. M.; Annabi, N. Local Immunomodulation Using an Adhesive Hydrogel Loaded with miRNA-Laden Nanoparticles Promotes Wound Healing. *Small Weinh. Bergstr. Ger.* **2019**, *15*, No. e1902232.

https://doi.org/10.1021/acsami.4c07612
ACS Appl. Mater. Interfaces 2024, 16, 47150−47162